===== **ACOUSTIC METHODS** =====

Determining the Type of Reflector from Amplitudes of Flares Reconstructed in Various Acoustic Schemes

E. G. Bazulin[a], *, A. Kh. Vopilkin[a], and D. S. Tikhonov[a]

[a] ECHO+ Scientific Production Association, Moscow, 123458 Russia

e-mail: bazulin@echoplus.ru

Abstract—Methods for recording and analyzing echo signals with the aim of determining the type of a reflector and sizing it have been developed in ultrasonic flaw detection. The digital antenna focusing (DFA) method makes it possible to reconstruct the image of the entire discontinuity boundary using echo signals reflected from the bottom of the test object taking into account wave type transformation. However, this approach is not always applicable in practice, since the shape of the test object bottom may be unknown. Using the features of the behavior of the reflection coefficient for various types of waves, it is possible to draw a conclusion about the reflector type only from normal beam images. Numerical and model experiments have confirmed the efficiency of the approach proposed.

1. INTRODUCTION

Determining the type of a reflector is an important problem in ultrasonic non-destructive testing, since the presence of cracks capable of rapid growth in the test object is extremely dangerous, and, vice versa, the presence of volumetric reflectors can insignificantly affect the strength properties of the test object. The method of digital focusing with an antenna array (DFA) makes it possible to reconstruct the image of the entire discontinuity boundary using echo signals reflected from the bottom of the test object, taking into account the transformation of the wave type [1−4]. However, this approach is not always applicable in practice, since the shape of the bottom of the test object may be unknown or it may be covered with corrosion pits. Therefore, the development of methods that allow making a well-founded judgment about the type of a reflector based solely on normal-beam echo signals remains relevant.

In the articles [5, 6], a method was proposed for determining the type of a reflector using the acoustic shape factor, calculated from the amplitudes of the pulses reflected from the upper and lower discontinuity. The disadvantage of this approach is that it is necessary to make an assumption, not always justified, that two echo signals being analyzed are scattered by the same reflector. To determine the type of a reflector it was proposed in the paper [7] to analyze the amplitudes of echo signals received by a special transducer designed to work with different types of waves reflected by the discontinuity. The low sensitivity and the need to develop and manufacture specialized two-element transducers make it difficult to apply this approach in practice. The article [8] proposes a method for determining the type of a reflector by analyzing the phase of reflector flares from complex normal-beam images reconstructed by the DFA method. However, for such a method to be reliably applied, it is necessary that echoes from the edges of the reflector do not overlap with other pulses. A similar principle for determining the type of a reflector was incorporated into the time of flight diffraction (TOFD) technology when it was developed [9].

Due to the small size of each element, antenna arrays allow one to work effectively with both longitudinal and transverse waves. The proposed method can be considered as a further development of the method in [7]; this should help solving the problem of determining the type of a reflector using its three images reconstructed by the C-SAFT method from one set of echo signals measured in the double scanning mode (full matrix capture (FMC)).
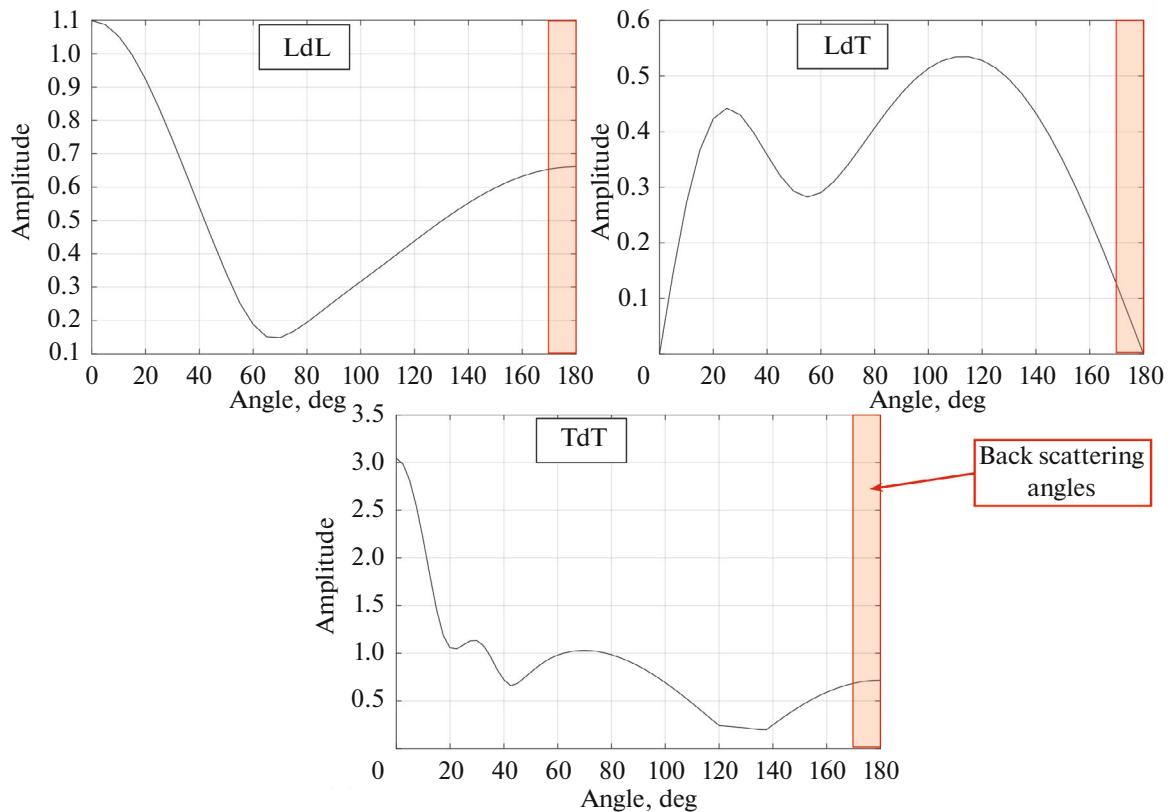
Fig. 1. Modulus of coefficients of scattering of incident plane wave with frequency 5 MHz by side-drilled hole 1 mm in diameter in steel specimen.

2. JUSTIFICATION OF THE PROPOSED METHOD

The proposed method for determining the type of a reflector is based on different behavior of the scattering coefficient for different types of waves on the bulk reflector and on the edges of the plane reflector.

2.1. Coefficient of Scattering by a Cylinder with Soft Boundary

To calculate the field of an incident plane harmonic wave scattered by a cylinder with soft boundary, one can use the exact analytical solution of the problem [10]. Figure 1 shows the values of the modulus of the coefficients of scattering by a side drilled hole (SDH) with a diameter of 1 mm in a steel sample for an incident plane wave with a frequency of 5 MHz. The rectangle with a red semitransparent filling shows the region corresponding to scattering in the direction opposite to the direction of the incident plane wave. It can be seen that when a longitudinal wave is scattered into a longitudinal wave (LdL) and when a transverse wave is scattered into a transverse wave (TdT), the values of the scattering indicatrix take on values greater than 0.5. However, for a longitudinal wave scattered into a transverse one (LdT), the values of the indicatrix of scattering in the opposite direction are less than 0.15 in the range of angles ±10 deg. A similar pattern is observed for the scattering of a transverse wave into a longitudinal one (TdL). The modulus of the reflection coefficients with wave type change is almost four times less than for the case with no wave type transformation.

2.2. Coefficient of Scattering of a Plane Wave by the Edge of a Semi-infinite Crack

In [11, 12], expressions are given for calculating the coefficient of reflection of a plane wave from the edge of a semi-infinite crack within the framework of the theory of geometric diffraction. Figure 2 shows the values of the moduli of the coefficients of scattering of a plane wave with a frequency of 5 MHz incident in the direction opposite to the plane-wave incidence direction by the edge of a crack in a steel specimen in the range of angles ±10 deg. The calculation results are shown for the incidence
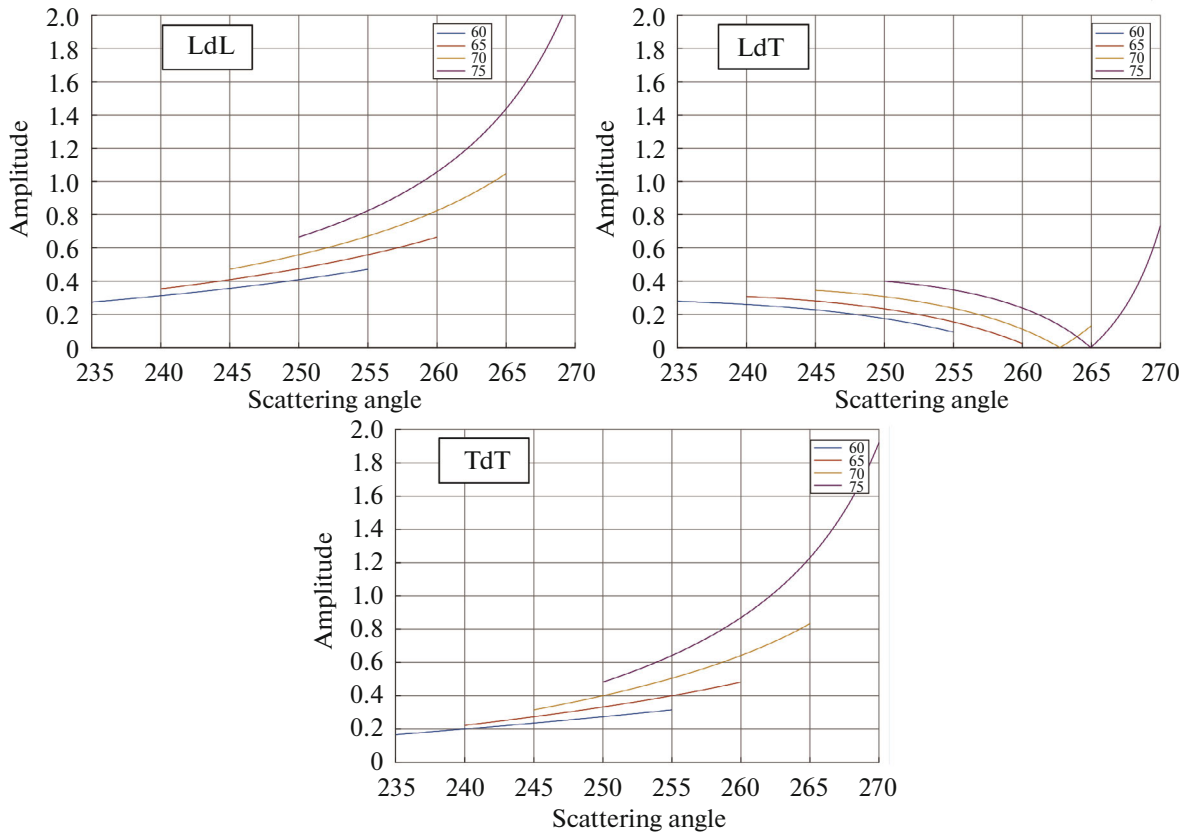
Fig. 2. Modulus of coefficients of backscattering of plane wave with frequency 5 MHz incident at angles of 65, 70, 75, and 80 deg to crack plane by its edges in steel specimen in angle range ±10 deg.

angles of 65, 70, 75, and 80 deg to the crack plane. Such angles correspond to the scattering of a plane wave by the upper edge of the crack. It is seen that for all types of scattering (LdL, LdT, and TdT) for the incidence angles of 65, 70, and 75 deg, the scattering coefficients differ from each other by approximately three times. However, with an increase in the angle of incidence to 80 deg, the scattering coefficient with no wave type transformation (LdL and TdT) can exceed the amplitude of the field scattered with wave type change (LdT) by an order of magnitude. Such angles are typical when the antenna array is far away from the reflector, as shown in Fig. 4. A similar pattern is observed for scattering by the bottom edge of a crack.

It should be noted that the amplitudes of the measured echo signals are determined not only by the scattering coefficients, the moduli of which are shown in Figs. 1 and 2, but also by the indices of refraction at the interface between the wedge and the test object and the distance from the points of emission and reception to the reflector. Integration over the surface of emission and reception when calculating echo signals will lead to their amplitudes differing from the amplitudes of the scattering coefficients.

3. NUMERICAL EXPERIMENTS

To test the proposed method for determining the type of a reflector, we used echo signals calculated by the CIVA software [13] according to the ray tube theory in a solid. It was assumed that the echo signals are recorded in the double scanning mode (Full Matrix Capture (FMC)) using an antenna array (5 MHz, 32 elements with dimensions of 0.55×10 mm and 0.05 mm gaps between element edges) installed either on a Rexolite® 35-degree wedge or on a Plexiglass® 20-degree wedge. The field was calculated at 5 points x_w on the wedge front face with the coordinates $-50, -40, -30, -20$, and -10 mm. Figure 3 shows the wedge at the farthest point with $x_w = -50$ mm.
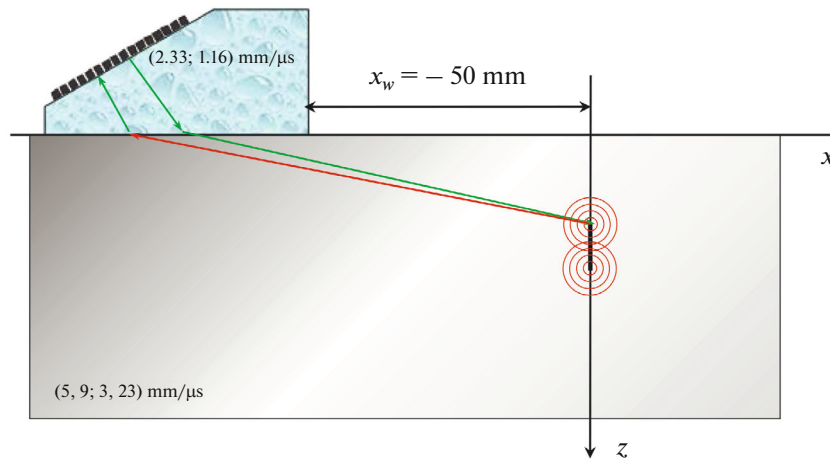
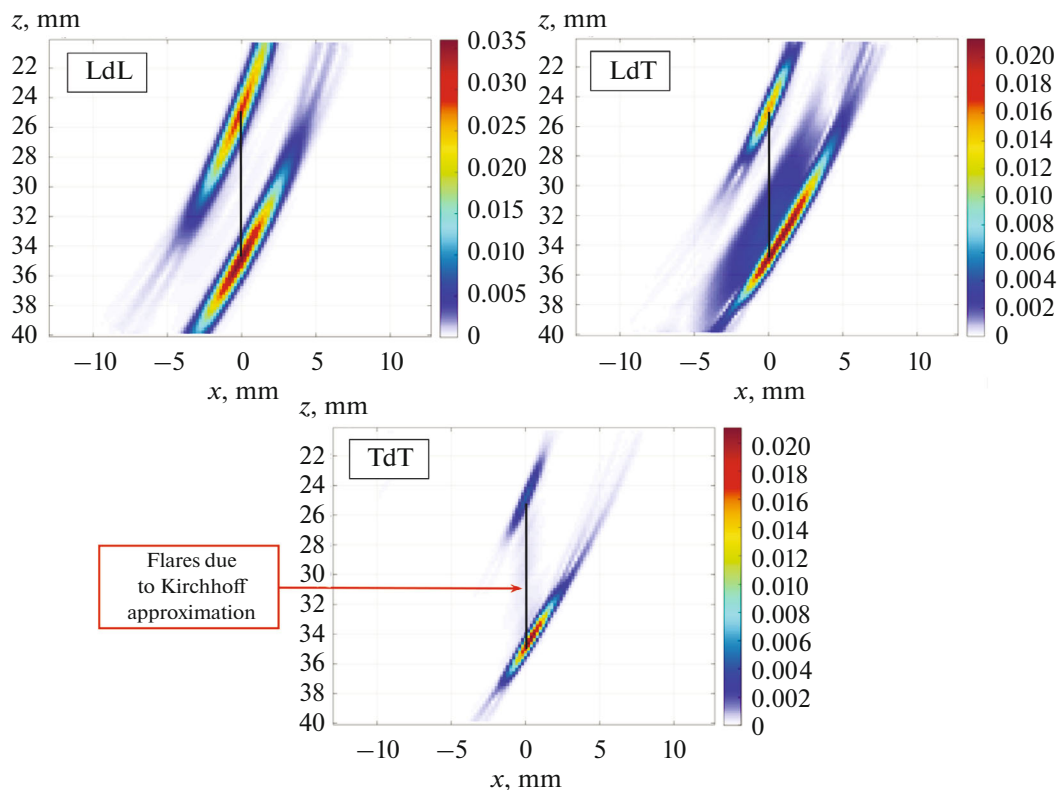**Fig. 3.** Schematic representation of the model for calculation with 35-degree wedge.

Fig. 4. Crack images according to three acoustic schemes LdL, LdT, and TdT with wedge located at point -30 mm.

3.1. Crack 10 mm High

We calculated echo signals scattered by a 10 mm high crack centered at the point $(0, 30)$ mm (shown in Fig. 3 by the thick black line) and echo signals scattered by two side-drilled holes 1 mm in diameter centered at the points $(0, 25)$ and $(0, 35)$ mm. The centers of the side-drilled holes have the same coordinates as the edges of the crack. The figure schematically shows the variant of a plane wave scattered by the upper edge of the crack according to the LdT scheme with wave type transformation. Longitudinal and transverse wave rays are indicated with green and red colors, respectively.
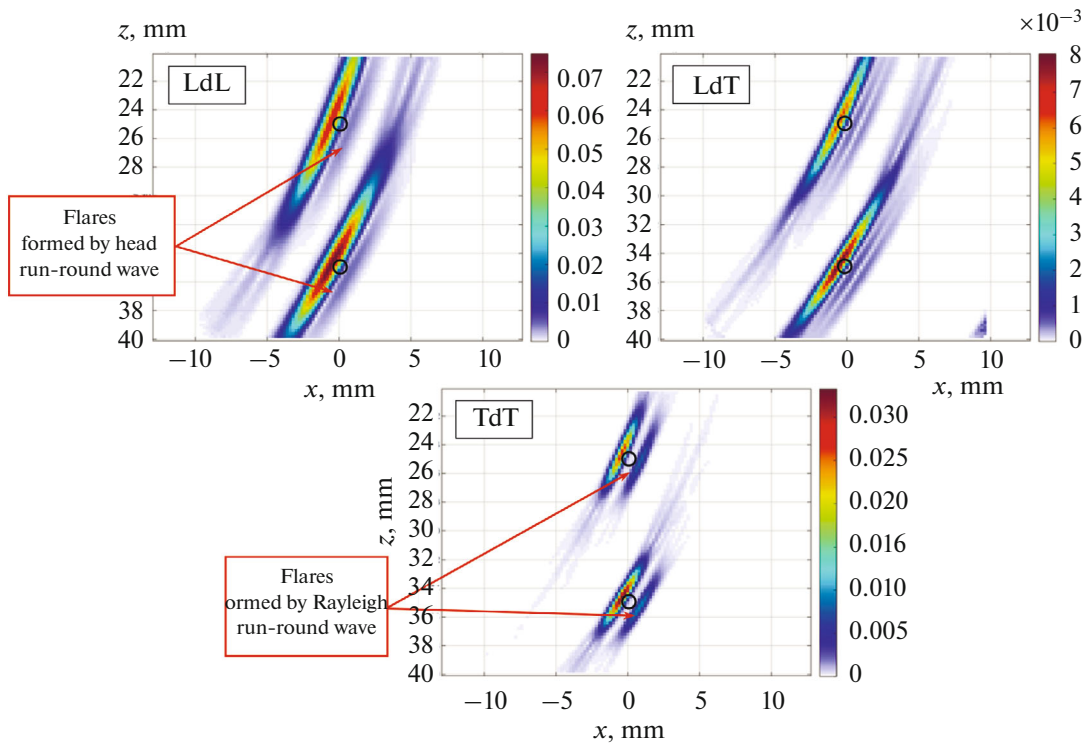
Fig. 5. Images of two side-drilled holes according to three acoustic schemes Ldl, LdT, and TdT.

The crack images were reconstructed from the calculated echo signals using the C-SAFT method [4] with three acoustic schemes LdL, LdT, and TdT. Figure 4 shows crack images obtained using a 35° Rexolite® wedge at the point −30 mm. The edges of a crack that is shown in the figures by the black line correspond to the flares reconstructed from the pulses diffracted by the crack edges, schematically represented by the red circles in Fig. 3. The amplitude of the flares can be judged by the amplitude of the color scale to the right of each figure. The image obtained in the TdT acoustic scheme supposedly shows diffuse crack surface reflections. The presence of reflections is explained by the use of Kirchhoff's approximation for calculating echo signals. Strictly speaking, having the images in Fig. 4, it is impossible to assert that a crack has been detected, since these flares can be formed by two volumetric reflectors of different diameters with coordinates close to the edges of the crack.

3.2. Two Side-Drilled Holes 1 mm in Diameter

Figure 5 shows the images of two side-drilled holes with a diameter of 1 mm obtained using a 35-degree Rexolite® wedge placed at the point −30 mm. It can be seen that the boundaries of the side-drilled holes (shown in the figures by black circles) correspond to flares, the amplitude of which can be judged by the amplitude of the color scale to the right of each figure. In the images, in addition to the flares of the side-drilled holes boundaries, one can observe flares formed by run-round/slipping (hereinafter referred to as run-round) pulses of a different nature. Theoretically, these flares can be considered as indirect signs of the presence of a volumetric reflector; however, when analyzing real images, these flares may be invisible against the background of interference or it will be difficult to unambiguously associate them with a flare due to the side-drilled hole boundary. Just as in the analysis of the images in Fig. 4, it is impossible to confidently solve the problem of determining the type of a reflector and to assert that two volumetric reflectors have been detected.

Images similar to those in Figs. 4 and 5 are also obtained when using a 20-degree Plexiglass® wedge. It is also impossible to determine the type of a reflector from these images with certainty, and therefore the images are not shown here.
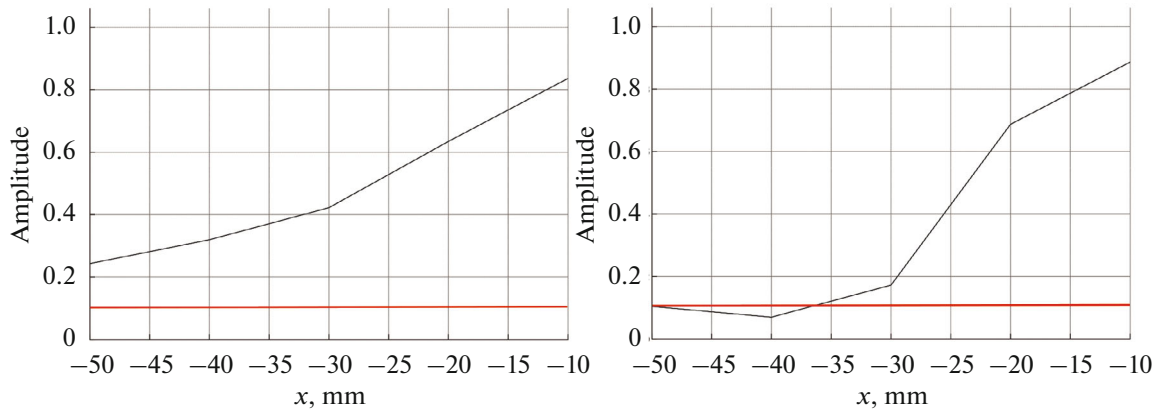
Fig. 6. Coefficient K calculated based on the flares of upper and lower crack edges for five positions of 35-degree Rexolite® wedge.

3.3. Method for Determining Reflector Type

The method for determining the type of a reflector is as follows. Three reflector images are reconstructed using the LdL, LdT, and TdT acoustic schemes from a set of echo signals once measured in the double scanning mode by the C-SAFT method to determine the amplitude of flares due to the reflectors. If we denote the amplitudes of the flares of one reflector in the images reconstructed according to different acoustic schemes by A_{LL}, A_{LT} and A_{TT}, then we can determine the coefficient

$$K = \frac{A_{LT}}{(A_{LL} + A_{TT})/2}. \tag{1}$$

If K is less than a certain level K_{level}, then we can assert that the flare corresponds to a volume-type reflector. If K is greater than the level K_{level}, then it can be argued that the detected reflector is a plane one. To do this, we need to determine the level K_{level}, which, strictly speaking, is a function of the depth h of the reflector and the wedge coordinates x_w.

Figure 6 shows the value of the coefficient K calculated based on the flares of the upper and lower edges of the crack for five positions of the 35-degree Rexolite® wedge. It can be seen that, with the exception of two points ($x_w = -40$ and -50 mm) for the lower edge of the crack, the coefficient K is greater than 0.1.

Figure 7 shows the value of the K coefficient calculated from the flares of the upper and lower edges of the crack for five positions of a 20-degree Plexiglass® wedge. It can be seen that, except for one point ($x_w = -50$ mm), the coefficient K is greater than 0.1 for the lower edge of the crack.

Figure 8 shows the value of the coefficient K calculated based on the flares of two side-drilled holes for five positions of a 35-degree Rexolite® wedge. It can be seen that the coefficient K is less than 0.1 for all wedge positions.

Figure 9 shows the value of the coefficient K for the flares of the upper and lower edges of the crack for five positions of the 20-degree Plexiglass® wedge. It can be seen that the coefficient K is less than 0.1 for all wedge positions.

Analysis of the graphs in Figs. 6—9 allows a conclusion that $K < 0.1$ for volumetric reflectors and $K < 0.1$ for plane reflectors, that is, $K_{level} = 0.1$. This is true when the wedge is placed at distances x_w greater than -40 mm.

4. MODEL EXPERIMENTS

Model experiments were carried out using the "AUGUR ART" DFA flaw detector developed and manufactured at Research and Production Center ECHO+ [14]. Echo signals were recorded by an antenna array (5 MHz, 32 piezoelectric elements with dimensions 0.55×10 mm, gap between the edges of piezoelectric elements 0.05 mm) mounted on a 35-degree Rexolite® wedge.
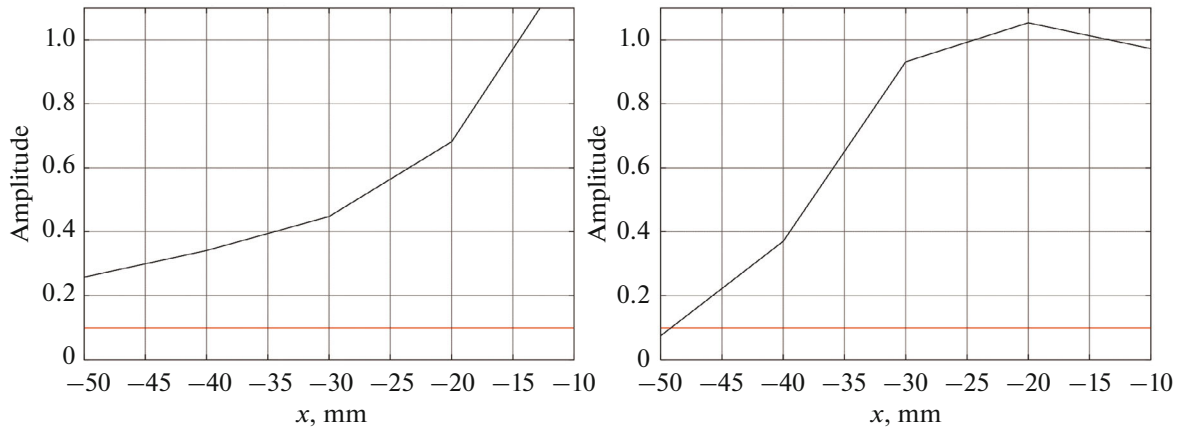
Fig. 7. Coefficient K of the flares of upper and lower crack edges for five positions of 20-degree Plexiglass® wedge.
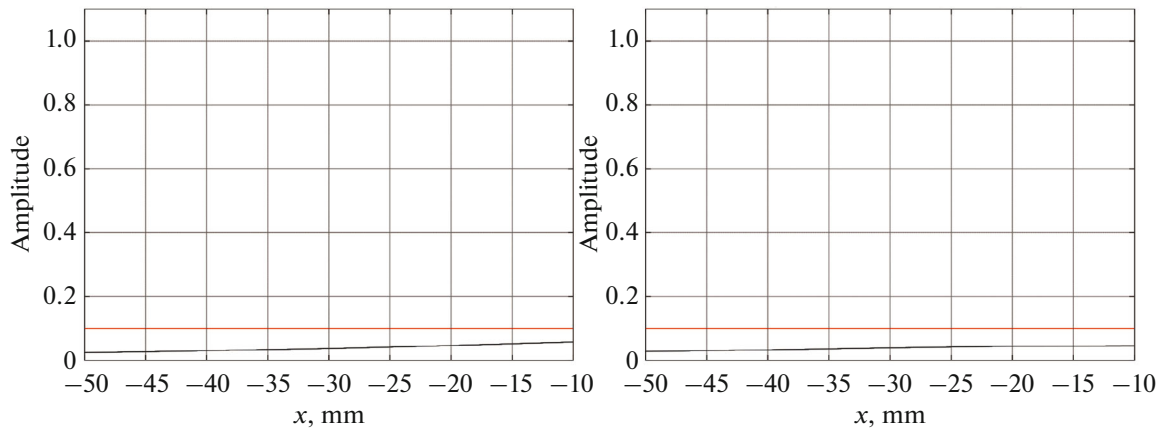

Fig. 8. Coefficient K of the flares of two side-drilled holes for five positions of 35-degree Rexolite® wedge.
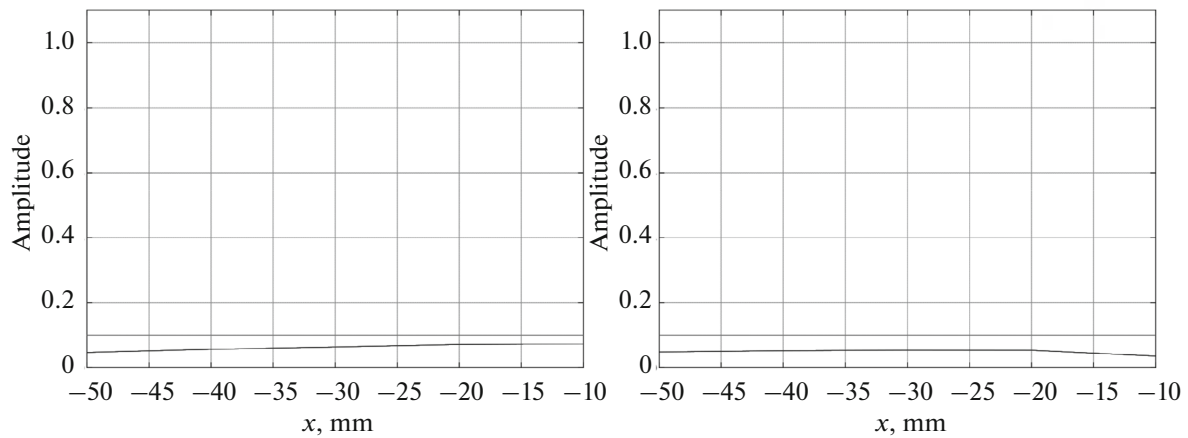

Fig. 9. Coefficient K value when applied to the flares of two side-drilled holes for five positions of 20-degree Plexiglass® wedge.
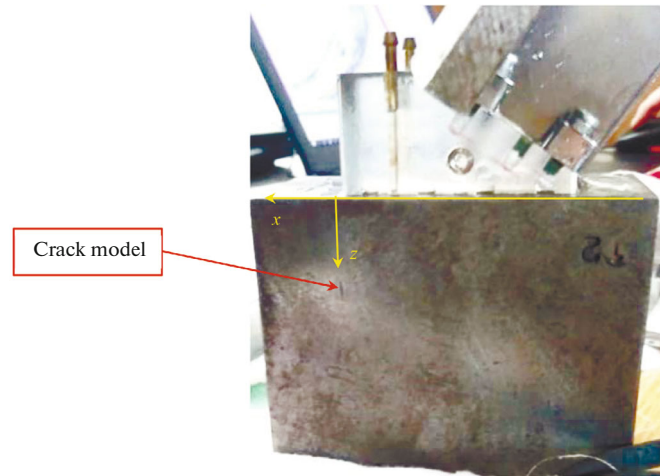
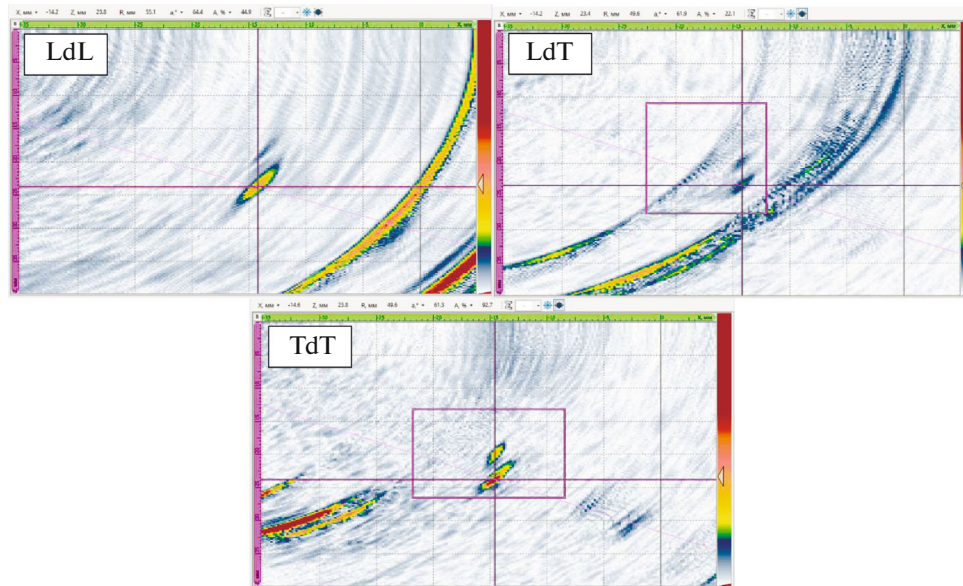**Fig. 10.** Photograph of specimen with 5-mm—high crack model.

Fig. 11. Image of 5-mm—high crack according to three acoustic schemes LdL, LdT, and TdT.

4.1. Crack 5 mm High

Measurements were taken for a sample with a 5 mm high crack model centered at a depth of 21.5 mm. The sample was manufactured as follows: a side-drilled hole was drilled in a workpiece made of grade 20 steel, then the workpiece was heated to 1000 degrees and placed in a press to completely collapse the hole into the model of a crack. A rectangular sample shown in Fig. 10 was fabricated from the workpiece obtained.

Figure 11 shows the crack images reconstructed by the C-SAFT method using three acoustic schemes LdL, LdT, and TdT from one set of measured echo signals. Just ass in the images in Fig. 4, the flares of the crack edges are clearly visible in all three images and correspond to the crack edges. The coefficient K for the flare of the lower boundary of the crack is approximately 0.32, and for the flare of the upper boundary the coefficient K is greater than 0.5, which allows us to conclude that a plane reflector has been detected with the dimensions that can be determined using two flares set at their maxima.
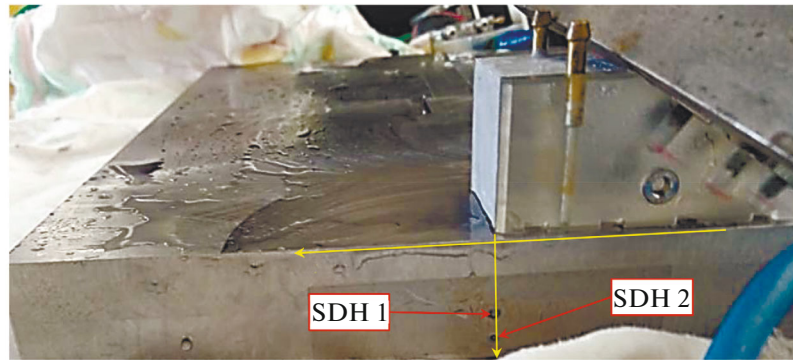
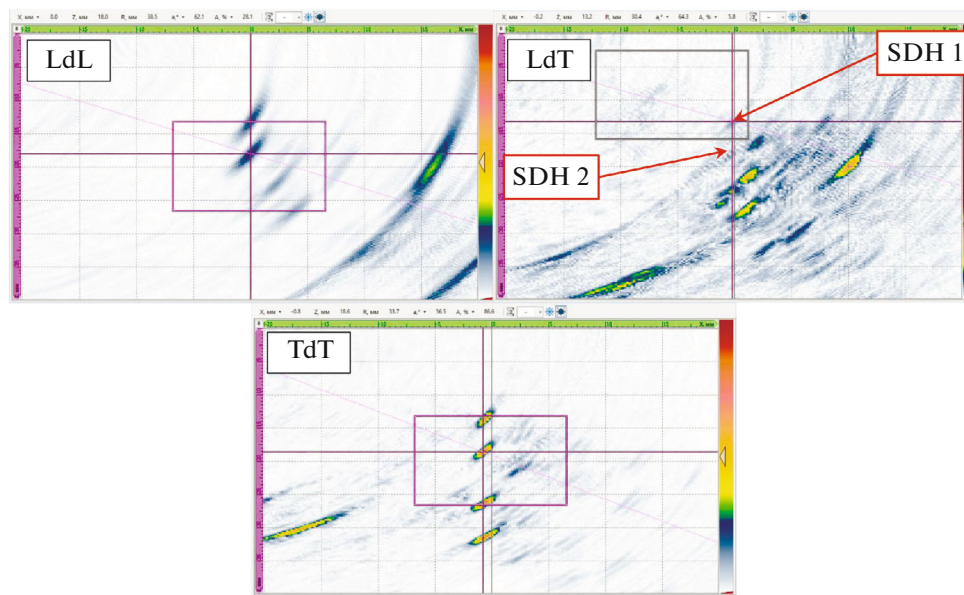**Fig. 12.** Photograph of specimen with SDH1 and SDH2 with diameter of 2 mm.

Fig. 13. Images of SDH1 and SDH2 with diameter of 2 mm according to three acoustic schemes LdL, LdT, and TdT.

4.2. Two Side-Drilled Holes with a Diameter of 2 mm

The measurements were carried out on a specimen made of grade 20 steel with two side-drilled holes (SDH) 2 mm in diameter drilled at depths of 13 and 18 mm (Fig. 12).

Figure 13 shows the images of SDH1 and SDH2 with a diameter of 2 mm, reconstructed using three acoustic schemes LdL, LdT, and TdT. Similar to Fig. 5, the amplitude of the flares of the side-drilled holes boundaries in the images reconstructed using the acoustic schemes LdL and TdT is almost an order of magnitude larger than the amplitude of the flares of the image reconstructed using the acoustic scheme LdT. The coefficient K for the flare of SDH1 and SDH2 is approximately 0.1. This suggests that the type of the detected reflector is volumetric.

5. CONCLUSIONS

The proposed method for determining the type of a reflector using the value of the coefficient K and the level $K_{level} = $ SDH 0.1 allows a justified assumption about the type of the detected reflector. The specific value of K_{level} should be determined when developing the object testing method. One should be aware that the proposed method does not give a 100% accurate answer to the question of the type of a reflector.

However, the analysis of the value of the coefficient K provides the operator with additional information to make a more accurate decision about the reflector type.

Note that the proposed method is suitable for working with phased array antennas (PAA). For this, it is necessary to obtain phased array images of the reflector for three laws of focusing according to the acoustic schemes LdL, LdT, and TdT. Naturally, the used phased array flaw detector should support the focusing mode, when radiation occurs on a longitudinal wave, and reception on a transverse wave (LdT).

ACKNOWLEDGMENTS

REFERENCES

1. Chatillon, S., Fidahoussen, A., Iakovleva, E., aand Calmon, P., Time of flight inverse matching re-construction of ultrasonic array data exploiting forwards models, *6th Int. Workshop NDT Signal Process.* (London, 2009).

2. Deleye, X., Hörchens, L., and Chougrani, K., Experimental comparison of wave-field based ultrasonic imaging with other advanced ultrasonic weld inspection techniques, *18th World Conf. Nondestr. Test.* (Durban, 2012).

3. Bazulin, E.G., Determination of the reflector type from an image reconstructed using echo signals measured with ultrasonic antenna arrays, *Russ. J. Nondestr. Test.,* 2014, vol. 50, no. 3, pp. 141−149.

4. Samokrutov, A.A. and Shevaldykin, V.G., Ultrasonic tomography of metal structures using the digitally focused antenna array method, *Russ. J. Nondestr. Test.,* 2011, vol. 47, no. 1, pp. 16−29.

5. Shcherbinskii, V.G. and Belyi, V.E., New informative sign of the nature of defects in ultrasonic testing, *Defektoskopiya,* 1975, no. 3, pp. 27−37.

6. Ushakov V.M., Bely V.E., Vopilkin A.Kh. Experimental study of acoustic fields of scattering of longitudinal and transverse waves on elliptical cavities, *Defektoskopiya,* 1987, no. 3, pp. 47−51.

7. Tsomuk, S.R., Experimental study of the ratio of the amplitudes of waves of various types as an identification sign of a defect, *Sb. trudov XI Vsesoyuznoy nauchno-tekh. konf. po nerazrushayushchim fizicheskim metodam i sredstvam kontrolya* (Proc. XI All-Union Sci. Tech. Conf. Nondest. Phys. Methods and Means of Testing), 1978, vol. 1, p. 134.

8. Bazulin, E.G., Vopilkin, A.Kh., et al. Analyzing the phase of DFA image for determining the type of detected reflector, *Russ. J. Nondestr. Test.,* 2019, vol. 55, no. 7, pp. 507−516.

9. Silk, M.G. and Lidington, B.H., The potential of scattered or diffracted ultrasound in the determination of crack depth, *Nondestr. Test.,* 1975, vol. 8, no. 6, pp. 146−151.

10. Golubev, A.S., Reflection of plane waves from a cylindrical defect, *Akust. Zh.,* 1961, vol. VII, no. 2, pp. 174−180.

11. Achenbach, J.D., Gautesen, A.K., and McMaken, H., *Ray Methods for Waves in Elastic Solids: With Applications to Scattering,* Boston: Pitman Adv. Publ. Progr., 1982.

12. Djakou, A.K., Darmon, M., Fradkin, L.J., and Chatillon, S., A system model for ultrasonic NDT based on the physical theory of diffraction (PTD), *Ultrasonics,* 2016, article ID 64:115-27.
https://doi.org//10.1016/j.ultras.2015.08.006

13. Official website of EXTENDE company. http://www.extende.com. Accessed January 7, 2021.

14. Official site of EKHO+ company. http://www.echoplus.ru. Accessed January 7, 2021.